# Supplementary material for

## Comparative study of X-ray charge density data on $CoSb_3$

Mette Stokkebro Schmøkel,[a] Lasse Bjerg,[a] Finn Krebs Larsen,[a] Jacob Overgaard,[a] Simone Cenedese,[c] Mogens Christensen,[a] Georg K. H. Madsen,[b] Carlo Gatti,[c]Eiji Nishibori,[d] Kunihisa Sugimoto,[e] Masaki Takata,[d,f] Bo Brummerstedt Iversen*[a]

[a]Center for Materials Crystallography, Department of Chemistry and iNANO, Aarhus University, Langelandsgade 140, DK-8000 Aarhus C. Denmark

[b]Department of Atomistic Modelling and Simulation, ICAMS, Ruhr-Universität, Bochum, Germany

[c]Istituto di Scienze e Tecnologie Molecolari del CNR (CNR-ISTM) e Dipartimento di Chimica, Università di Milano, via Golgi 19, I-20133, Milano, Italy[d] RIKEN SPring-8 Center. RIKEN, 1-1-1, Kouto, Sayo-cho, Sayo-gun, Hyogo 679-5148, Japan

[e]Japan Synchrotron Radiation Research Institute I-I-I, Kouto, Sayo-cho, Sayo-gun, Hyogo 679-5198, Japan.

### *Data collection and data treatment*

*Aarhus, Huber*

Multifaceted $CoSb_3$ crystals were prepared by chemical vapor transport deposition with chlorine gas as transport agent. A rather spherical crystal of approximate radius of 60 µm and morphology with (100) and (110) forms best developed was mounted on a type 512 Huber four-circle diffractometer equipped with a type 202 Displex refrigerator operated with the crystal cooled to 10.5(5) K (Henriksen *et al.*, 1986). Graphite-monochromatized Ag $K_\alpha$ radiation was employed for data collection. The unit cell was determined by least-squares fitting of the setting angles of 24 well-spaced reflections with $21^o<|2\theta|<68^o$ with some reflections centered at both positive and negative values of $2\theta$. Half a sphere of data was collected out to $\sin\theta/\lambda_{max}$=1.2337 $Å^{-1}$, some parts more than once. 37175 reflections were collected, measuring three standards every 50 reflections with periodic recentering and update of orientation matrix. The standards showed a decay of about 5% in intensity over the 5 months data collection period. Integrated intensities were extracted from the raw data by the use of the profile-analysis program COLL5N, based on the minimization of $\sigma(I)/I$ (Lehmann & Larsen, 1974) normalized to the decay of the standard reflection intensities. A Gaussian absorption correction with $\mu$=12.72 $mm^{-1}$ gave transmissions

$T_{min}$=0.21 and $T_{max}$=0.30. 33077 reflections collected in the most steady periods were accepted, sorted and averaged. Outliers in the averaging of equivalent reflections were rejected to give 1071 unique reflections. The agreement of equivalents was $R_{int}$(I)=0.032.

*APS05*

A multifaceted $CoSb_3$ crystal from the same batch as the crystal used at the Aarhus Huber experiment was selected for the synchrotron data collection experiments. The crystal had a maximum diameter of ~10 μm and was mounted on the tip of a fine-pointed glass fibre glued to a brass pedestal. which was placed on the goniometer of a Huber fourcircle diffractometer at the ChemMatCARS beam line at the Advanced Photon Source (APS), Argonne National Laboratory, USA. The crystal was cooled to 15(2) K in a cold He stream. The data collection was done in φ-scan mode with steps of 0.3° (X s exposure) and fixed ω and χ angles. The detector distance was 5.5 cm. The diffracted intensity was recorded with a SMART6000 charge-coupled device (CCD) detector mounted on the 2θ-arm of the diffractometer. The maximum resolution was 1.26 $Å^{-1}$, and a total of 16741 reflections were integrated with SAINT$^+$ v6.45A. After integration, the data were corrected for oblique incidence into the CCD detector (Wu *et al.*, 2002). Data were subsequently averaged and corrected for absorption with SORTAV. In the multipole modeling of the data, only reflections measured more than twice were included in the refinements.

APS08

The same crystal as used in 2005 is used for this experiment at the same beam line, with an upgraded CCD-detector (Bruker Apex2). Data was collected using φ-scans of 0.3° steps. The crystal temperature was again kept at 15 K using a Helijet. The resolution of this data set was 1.61 $Å^{-1}$, with an internal agreement of 4.3% for the 14310 reflections integrated using SAINT$^+$. The data were averaged using SORTAV. The correction for oblique incidence was again carried out in a local program as above, taking the different wavelength of 0.4428 Å into account, for which a transmission factor at perpendicular incidence of 0.5273 is known.

*SPring8*

For further details concerning the SPring8 data collection and processing we refer to our communication, Schmøkel *et al.* (2013).

**References**


Henriksen, K., Larsen, F. K., & Rasmussen, S. E. (1986). *J. Appl. Cryst.* **19**, 390-394.

Lehmann, M. S. & Larsen, F. K. (1974). *Acta Cryst. A* **30**, 580-584.

Schmøkel, M., Bjerg, L., Overgaard, J., Larsen, F. K., Madsen, G., Sugimoto, K., Takata, M., Iversen & B. B. (2013) *Angew. Chem. Intl. Ed.* **52**, 1503-1506.

Wu, G.; Rodrigues, B. L.; Coppens, P. J. Appl. Crystallogr. 2002, 35, 356-359.

**Table S1.** Refinement results for all full experimental data sets. $s=\sin\theta/\lambda$. The $\kappa$-parameters have been fixed (KKRMM) at the values obtained from the refinement of the full theoretical data set.

| | **SPring8** | **APS05** | **APS08** | **Aarhus** | **Powder** |
|---|---|---|---|---|---|
| $\sin\theta/\lambda$ (Å$^{-1}$) | 1.667 | 1.268 | 1.615 | 1.234 | 1.805 |
| $R(F^2)$ | 1.35 % | 2.35 % | 2.43 % | 3.49 % | 2.34 % |
| $\pm\Delta\rho$ (e/Å$^3$) | 8.42/-2.10 | 7.72/-2.66 | 6.46/-2.24 | 11.59/-4.78 | 17.78/-7.79 |
| $\pm\Delta\rho$ ($\sin\theta/\lambda$<0.8 Å$^{-1}$) | 1.76/-0.48 | 3.25/-0.64 | 2.71/-0.71 | 3.21/-2.12 | 1.56/-1.00 |
| $N_{used}$ ($I>3\sigma$) | 2154 | 902 | 2097 | 1033 | 2356 |

**Figure S1.** plots of the variation of scale factor ($\Sigma F_o^2/\Sigma F_c^2$) with resolution (for data averaged within 0.05 $Å^{-1}$ intervals) from the multipole refinements of the reduced experimental and theoretical data sets.

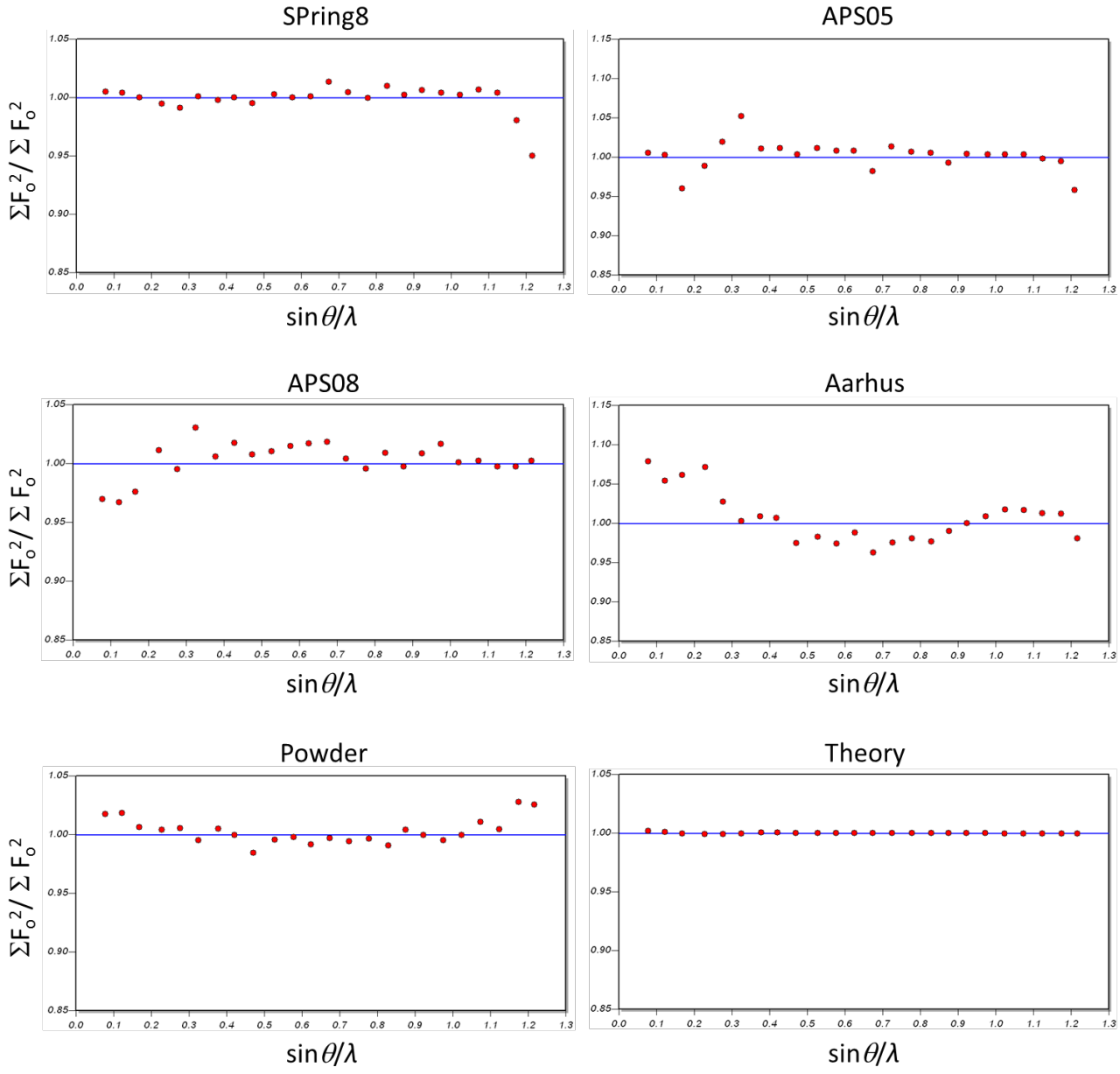

**Figure S2.** Normal probability plots from the multipole refinements of the reduced experimental data sets.

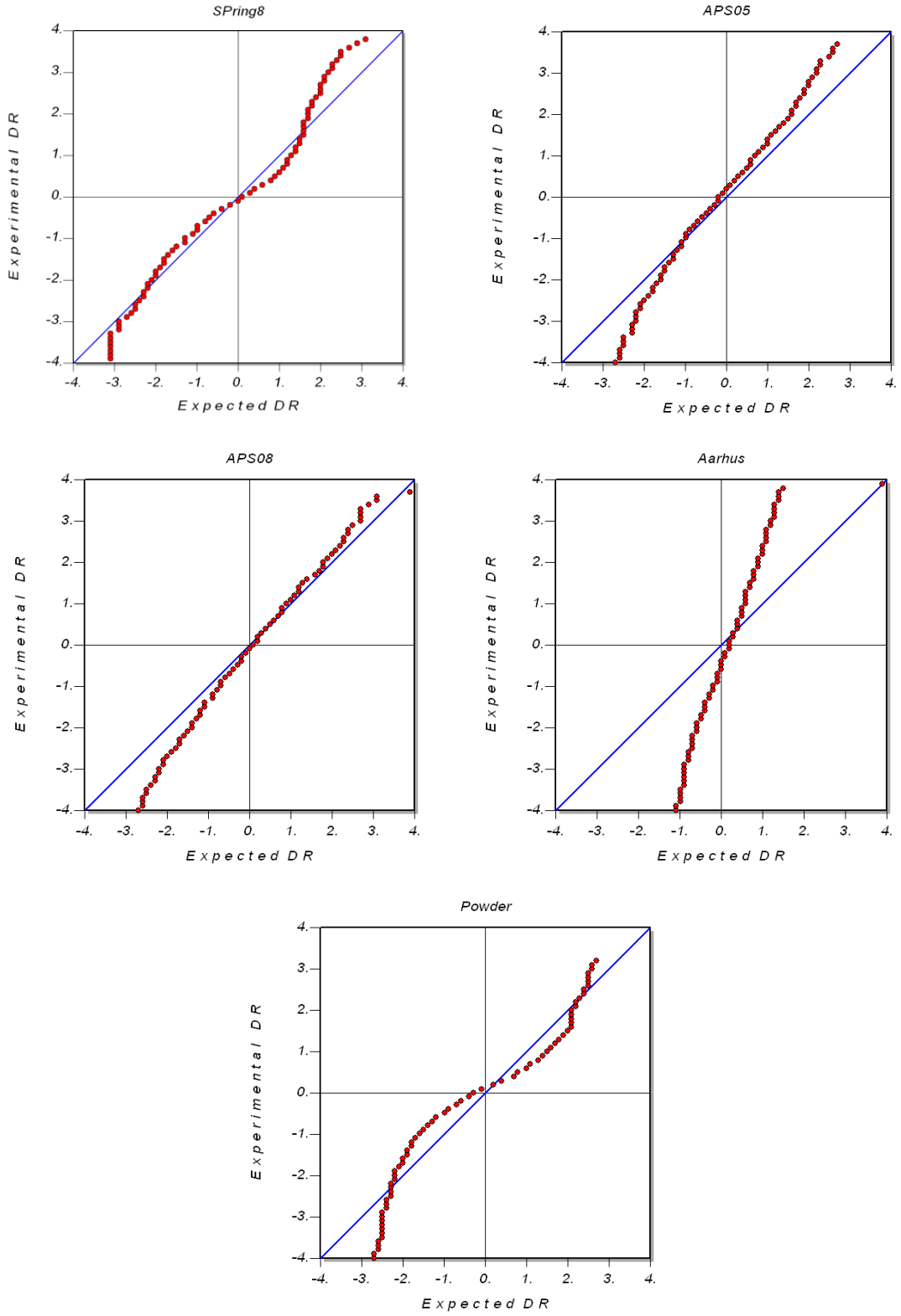

**Figure S3.** Residual density plots in the plane of the $Sb_4$ unit for reduced data sets: a) SPring8 data, b) APS05, c) APS08, d) Aarhus, e) Powder. All reflections present in the *reduced* data sets are included in all cases. The step size is 0.1 e/Å$^3$. Full, blue contours are positive. Dashed, red contours are negative.

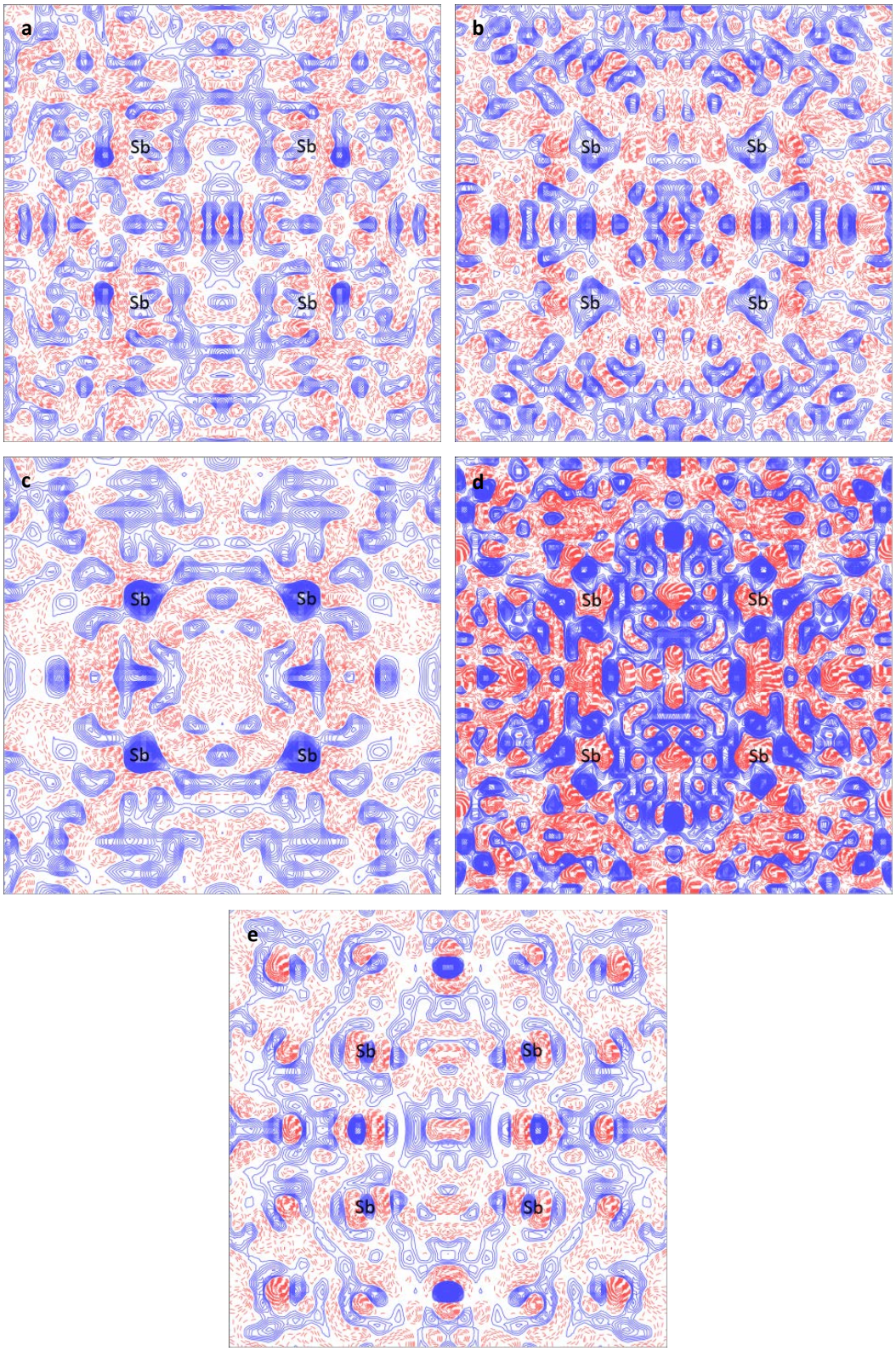

**Figure S4.** Contour plots of the negative Laplacian in the plane of the $Sb_4$ unit for the static ED obtained for all reduced data sets: a) SPring8, b) APS05, c) APS08, d) Aarhus, e) Powder, f) Theoretical data. Reflections up to 1.2337 $Å^{-1}$ are included for all data sets.

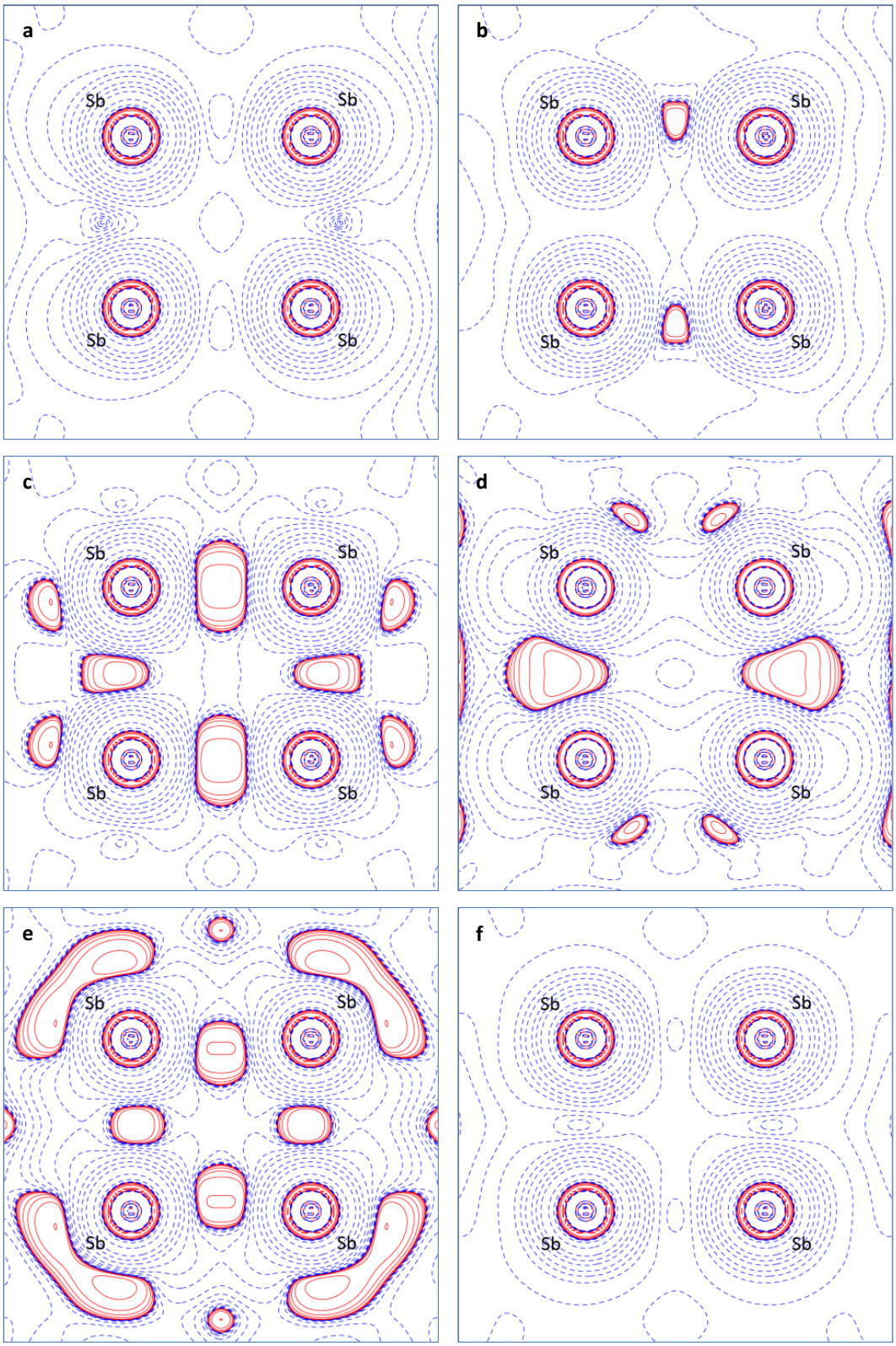

**Figure S5.** The highest residual peak is found at the cage centre positions at (0,0,0). Several causes for this extremely high peak have been investigated. Initially the feature was suspected to be due to the presence of a small amount of impurity atoms. Chlorine was judged to be the most likely candidate since the synthesis of the compound was made with $Cl_2$ as a transport agent.[1] However, as seen from the EDX spectrum recorded for a $CoSb_3$ crystal (top), only trace amounts of Cl are found apart from Co and Sb. No reliable quantization of the stoichiometry of the elements can be obtained. A more qualified guess is that the residual originates from error accumulation at a high-symmetry, high-multiplicity position (the (0,0,0) site has *m-3* point symmetry and a multiplicity of 24) (Cruickshank & Rollett, 1953. Rees, 1976). This is supported by plots of the residual density at the (0,0,0) position for the SPring8 multipole refinement (bottom left: isocontour levels are at ±1 e/Å$^3$; bottom middle: relief plot of the residual density; $\sin\theta/\lambda$<0.8 Å$^{-1}$). Also, a relief plot of the electron density at (0,0,0) obtained from Fourier transformation of $F_{obs}$ is shown (bottom, right; the Sb atoms are seen at the corners). A cut-off of $\rho_{max}$ = 40 e/Å$^3$ has been used for the latter.

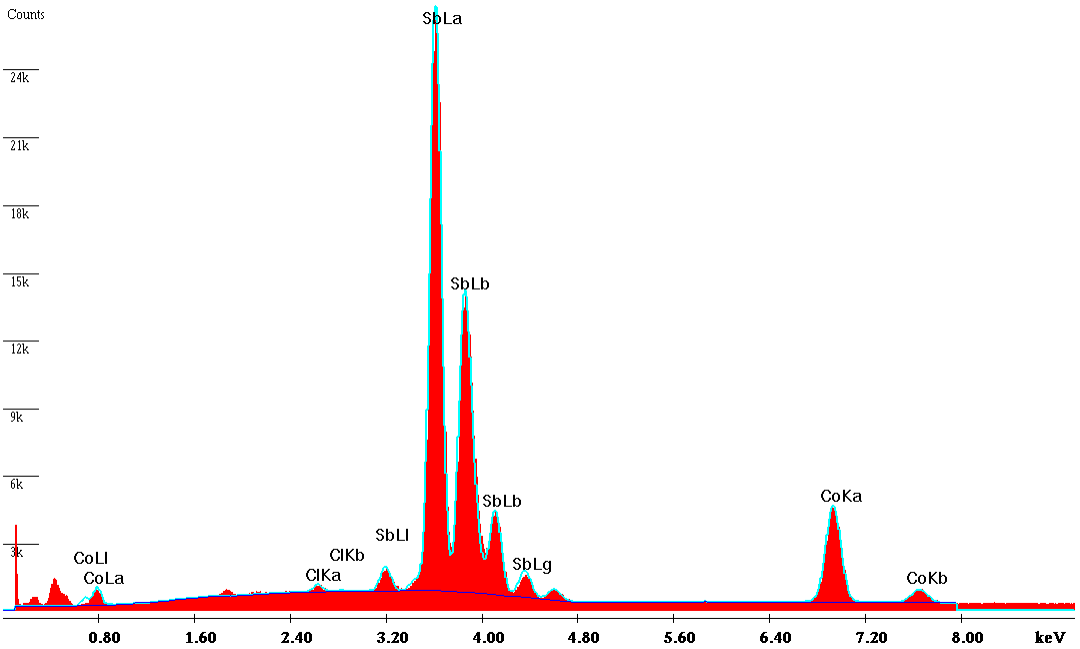


[1] The slightly higher unit cell reported from the use of $I_2$ instead of $Cl_2$ in gas transport synthesis of the compound seemed to support the idea of inclusion of a small amount of the gas in the structure (Schmidt *et al.*, 1987).

**Table S2.** Atomic positions and ADPs: Theory, SPring8 KKRMM and SPring8 UMM.

| | | Theory | SPring8 KKRMM | SPring8 UMM |
|---|---|---|---|---|
| | ***x, y, z*** | 0.25 | 0.25 | 0.25 |
| **Co** | $U_{11}$ | - | 0.00248(1) | 0.00248(1) |
| | $U_{12}$ | - | 0.00005(1) | 0.00005(1) |
| | ***x*** | 0 | 0 | 0 |
| | ***y*** | 0.33522 | 0.335221(4) | 0.335221(4) |
| | ***z*** | 0.15786 | 0.157861(4) | 0.157860(4) |
| **Sb** | $U_{11}$ | - | 0.00222(1) | 0.00221(1) |
| | $U_{22}$ | - | 0.00266(1) | 0.00265(1) |
| | $U_{33}$ | - | 0.00240(1) | 0.00239(1) |
| | $U_{23}$ | - | 0.00010(1) | 0.00010(1) |

**Table S3. a)** Monopole populations, radial parameters and net atomic charges from multipole refinement: Theory, SPring8 KKRMM and UMM.

| | Atom | $P_{val}$ | $\kappa$ | $P_{00}$ | $\kappa'$ | Net charge |
|---|---|---|---|---|---|---|
| **Theory** | Sb | 4.984(1) | 0.9790(4) | 0 | 0.803(3) | +0.016(1) |
| | Co | 7.047(4) | 0.9916(3) | 0 | 1.020(4) | -0.047(4) |
| **SPring8 KKRMM** | Sb | 4.85(4) | 0.979001 | 0.000 | 0.803150 | +0.15(4) |
| | Co | 7.5(1) | 0.991563 | 0.000 | 1.019832 | -0.5(1) |
| **SPring8 UMM** | Sb | 4.97(7) | 1.09(3) | 0.000 | 0.69(6) | +0.03(7) |
| | Co | 7.1(2) | 1.02(1) | 0.000 | 0.74(7) | -0.1(2) |

**Table S3. b)** Dipole population parameters: Theory, SPring8 KKRMM and SPring8 UMM.

| | Atom | $D_{11+}$ | $D_{11-}$ | $D_{10}$ | $\kappa'$ |
|---|---|---|---|---|---|
| **Theory** | Sb | 0.007(2) | -0.013(3) | 0 | 0.803 |
| | Co | 0 | 0 | 0 | 1.020 |
| **SPring8 KKRMM** | Sb | 0.1(1) | 0.1(1) | 0 | 0.803 |
| | Co | 0 | 0 | 0 | 1.020 |
| **SPring8 UMM** | Sb | 0.27(30) | 0.30(36) | 0 | 0.694 |
| | Co | 0 | 0 | 0 | 0.736 |

**Table S3. c)** Quadrupole population parameters: Theory, SPring8 KKRMM and SPring8 UMM.

| | Atom | $Q_{20}$ | $Q_{21+}$ | $Q_{21-}$ | $Q_{22+}$ | $Q_{22-}$ |
|---|---|---|---|---|---|---|
| **Theory** | Sb | 0.109(2) | 0 | 0 | -0.001(3) | 0.035(2) |
| | Co | 0.011(0) | 0 | 0 | 0 | 0 |
| **SPring8 KKRMM** | Sb | 0.1(1) | 0 | 0 | -0.2(1) | -0.3(3) |
| | Co | -0.001(26) | 0 | 0 | 0 | 0 |
| **SPring8 UMM** | Sb | 0.28(31) | 0 | 0 | -0.04(22) | -0.31(53) |
| | Co | 0.013(35) | 0 | 0 | 0 | 0 |

**Table S3. d)** Octupole population parameters: Theory, SPring8 KKRMM and SPring8 UMM.

| | Atom | $O_{30}$ | $O_{31+}$ | $O_{31-}$ | $O_{32+}$ | $O_{32-}$ | $O_{33+}$ | $O_{33-}$ |
|---|---|---|---|---|---|---|---|---|
| **Theory** | Sb | 0 | -0.138(3) | -0.150(3) | 0 | 0 | 0.060(3) | -0.073(3) |
| | Co | 0 | 0 | 0 | 0 | 0 | 0 | 0 |
| **SPring8 KKRMM** | Sb | 0 | -0.2(2) | -0.06(11) | 0 | 0 | 0.2(1) | -0.01(8) |
| | Co | 0 | 0 | 0 | 0 | 0 | 0 | 0 |
| **SPring8 UMM** | Sb | 0 | -0.36(27) | -0.42(22) | 0 | 0 | 0.46(23) | 0.07(14) |
| | Co | 0 | 0 | 0 | 0 | 0 | 0 | 0 |

**Table S3. e)** Hexadecapole population parameters: Theory, SPring8 KKRMM and SPring8 UMM.

| | Atom | $H_{40}$ | $H_{41+}$ | $H_{41-}$ | $H_{42+}$ | $H_{42-}$ | $H_{43+}$ | $H_{43-}$ | $H_{44+}$ | $H_{44-}$ |
|---|---|---|---|---|---|---|---|---|---|---|
| **Theory** | Sb | 0.045(3) | 0 | 0 | 0.017(2) | 0.024(2) | 0 | 0 | 0.062(2) | 0.011(3) |
| | Co | 0.081(0) | 0 | 0 | 0 | 0 | -0.146(1) | 0.017(0) | 0 | 0 |
| **SPring8 KKRMM** | Sb | -0.1(2) | 0 | 0 | -0.01(13) | 0.05(13) | 0 | 0 | 0.03(16) | 0.003(60) |
| | Co | 0.10(3) | 0 | 0 | 0 | 0 | -0.16(3) | 0.03(3) | 0 | 0 |
| **SPring8 UMM** | Sb | -0.14(30) | 0 | 0 | 0.00(18) | 0.08(22) | 0 | 0 | 0.01(23) | -0.10(9) |
| | Co | 0.14(4) | 0 | 0 | 0 | 0 | -0.22(4) | 0.053(34) | 0 | 0 |

**Figure S6.** Contour plots of the static deformation density in the plane of the $Sb_4$ unit for the theoretical data (left) and the SPring8 data fitted with the KKRMM model (middle) and the UMM model (right). The contour step size is 0.05 e/Å$^3$. Full, blue contours are positive. Dashed, red contours are negative. Black dotted lines are zero contours.

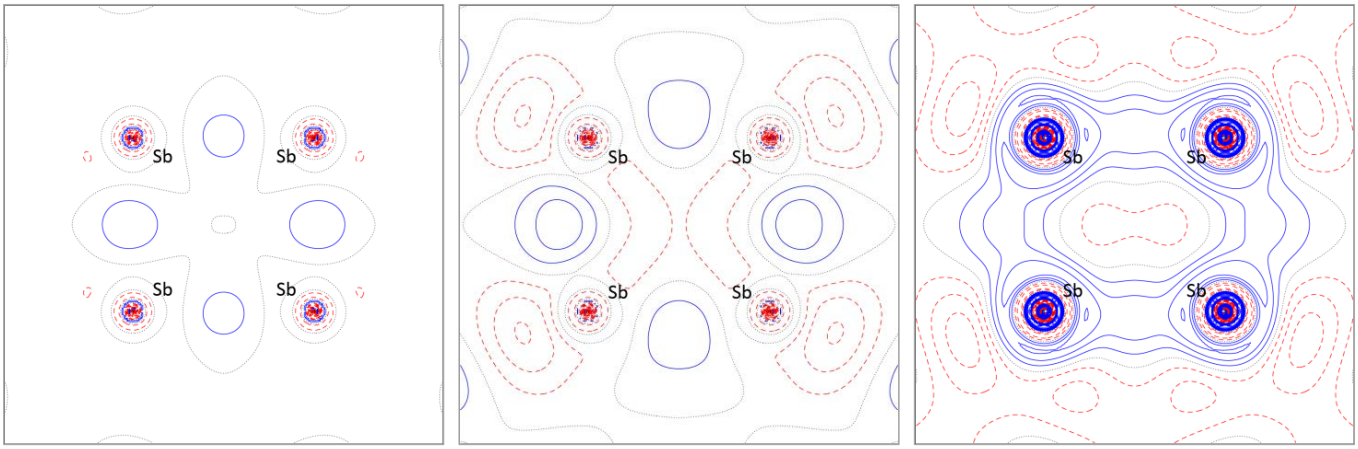


**Figure S7.** Contour plot of the Laplacian in the plane of the $CoSb_4$ unit for the theoretical data (left), the SPring8 data fitted with the KKRMM, (middle) and the SPring8 data fitted with the UMM (right). Positive contours are plotted with blue, dashed lines, negative contours with full, red lines.

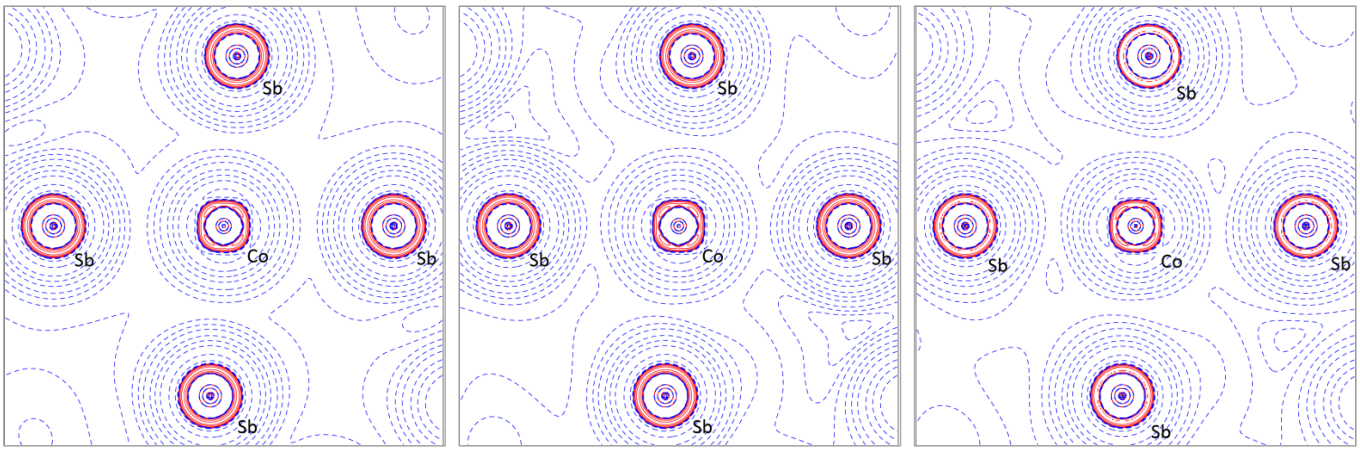

**Figure S8.** The Laplacian plotted along the direction of the Sb-Sb and Sb-Co interactions and along the bond path for the electron density obtained from multipole fitting to the data. Left: Sb-Sb long, middle: Sb-Sb short, right: Sb-Co. Blue line: Laplacian profile based on the multipole fitted (MM) electron density. Red line: Laplacian profile based on the IAM electron density. Black line: the Laplacian based on the multipole fitted density along the bond path (BP). The stars mark the position of the bcp for the MM electron density, and the circle marks the position of the bcp for the direct theoretical density.

a) Theory

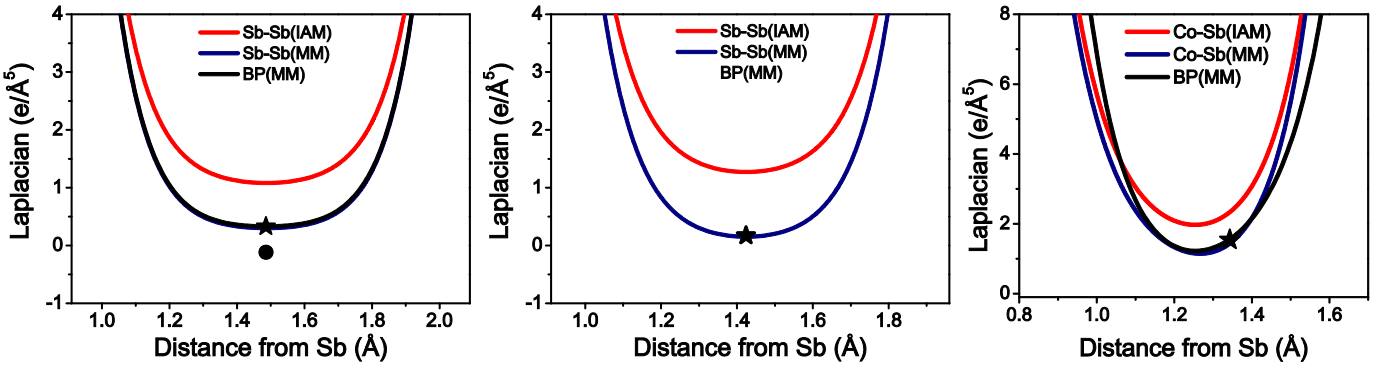


b) SPring8, KKRMM

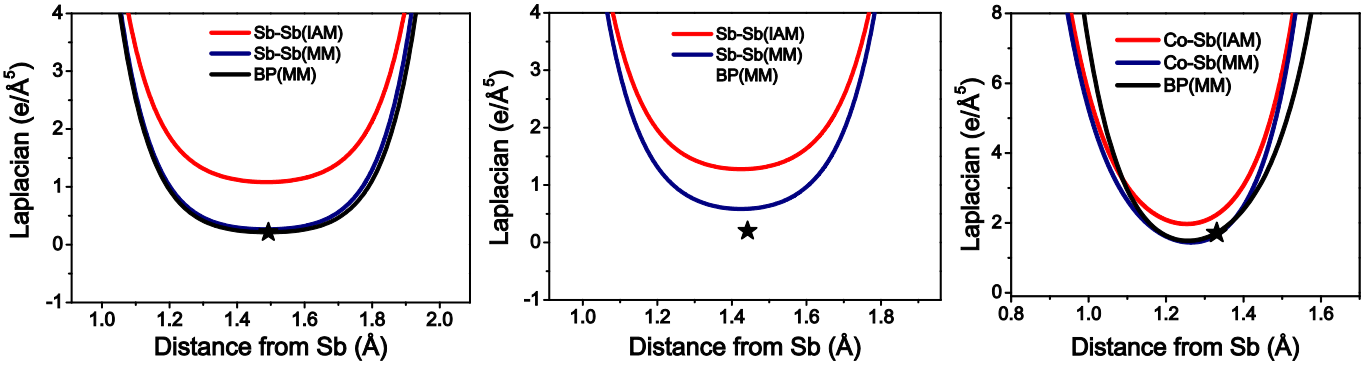


c) SPring8, UMM

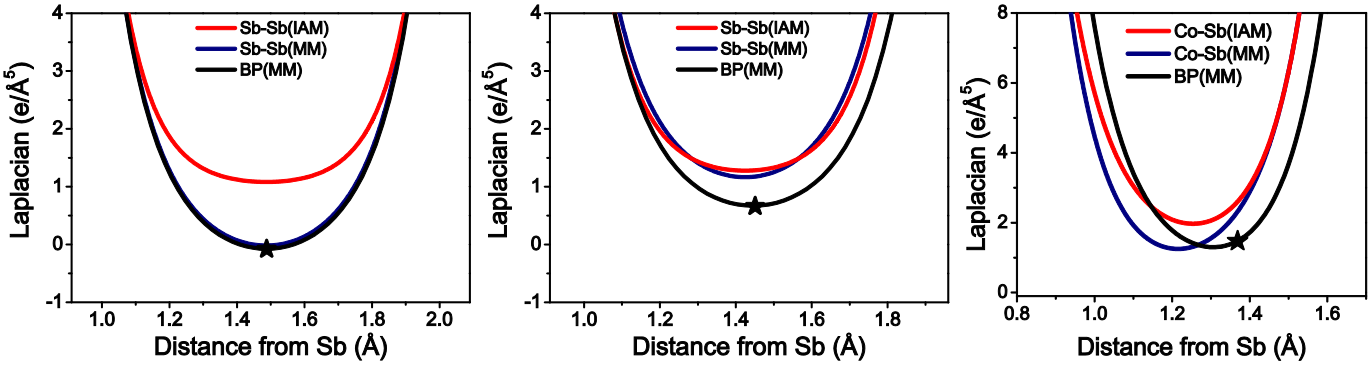

***Comparison of different models***

Five different models, each treating the valence on the cobalt atom differently, have been refined against the theoretical and the SPring8 data. The results are shown in Table S4, a)-c). For the refinement against the SPring8 data, the five models have been applied both for the UMM and KKRMM approach. In all cases a Co(3*d*) population of 7 *e* or slightly higher is found, and for the SPring8 data $Q_{ATB}$(Co) is always negative. Details on the various models are given below.

1) *Model 1:* This is the 'standard' model which is used in the main paper containing the full topological analysis. The 4*s* electrons on Co are treated as part of the core. Only the seven 3*d* electrons on Co are treated as valence. Single-zeta Slater-type radial functions are used for the valence deformation density of Co. Using HF radial functions, as otherwise recommended (Macchi & Sironi, 2003) does not significantly improve the refinement in terms of *R*-factors and residual density peaks.

2) *Model 2:* The 4*s* and 3*d* shells on Co are both treated as valence simultaneously (i.e. as one valence). This means that the radial functions correspond to a weighted average of 4*s* and 3*d* type functions and that the initial valence population is 7 *e*. Single-zeta Slater-type radial functions are used for the valence deformation density of Co. Due to the large difference in the radial dependence of the 4*s* and the 3*d* shells this is not an optimal approach and, though included, this model is not considered as an option.

3) *Model 3:* The two 4*s* electrons on Co are removed from the core and moved into the 3*d* shell so this now contains nine electrons (i.e. the initial valence population is 9 *e*) that are treated as valence. HF (3*d* type) radial functions are used for the valence deformation density of Co.

4) *Model 4:* The two 4*s* electrons are removed from the Co core and are together with one Co 3*d* electron moved to the Sb 5*p* shell leading to a starting $5s^2 5p^4$ valence configuration on Sb and an initial valence population on Co of 6 *e*. HF radial functions are used for the valence deformation density on Co.

5) *Model 5:* Two monopoles are used for Co: one corresponding to the 3*d* shell and another to the 4*s* shell. HF radial functions are used for both Co valence deformation densities. The odd-order multipoles are assigned to the 4*s* shell and the even order multipoles to the 3*d* shell. Sb is treated as in Model 1-3 with an initial $5s^2 5p^3$ valence configuration. Co is treated as in Model 1 but including independent refinement of the population and $\kappa$ of the Co(4*s*) shell.

**Table S4.a:** Results from multipole refinements against the theoretical data. The refinements are performed on *F* with the scale factor fixed at a value of 1. Five different models are tested all with freely refined $\kappa$ and $\kappa'$ (UMM).

| **Theory, UMM** | **Model 1** | **Model 2** | **Model 3** | **Model 4** | **Model 5** |
|---|---|---|---|---|---|
| $R(F)$ | 0.04 % | 0.03 % | 0.04 % | 0.03 % | 0.02 % |
| $\pm\Delta\rho$ (e/Å$^3$) | -0.159/0.151 | -0.156/0.152 | -0.195/0.163 | -0.129/0.155 | -0.14/0.15 |
| $\pm\Delta\rho^{2nd}$ (e/Å$^3$) | 0.06/-0.09 | 0.08/-0.09 | 0.05/-0.11 | 0.06/-0.12 | 0.06/-0.02 |
| $\kappa$ (Co, 4s) | - | - | - | - | 0.988(4) |
| $\kappa$, $\kappa'$ (Co) | 0.992, 1.020(4) | 0.991, 1.367(5) | 0.998, 1.012(9) | 0.999, 1.015(8) | 0.993, 1.036(5) |
| $\kappa$, $\kappa'$ (Sb) | 0.979, 0.803(3) | 0.979, 0.798(3) | 0.951, 0.747(3) | 0.965, 0.757(2) | 0.974, 0.791(3) |
| $P_{val}$(Co), $P_{val}$(4s) | 7.047(4) | 9.062(5) | 7.021(7) | 7.011(6) | 7.049(4), 1.62(3) |
| $P_{val}$(Sb) | 4.984(1) | 4.979(2) | 5.659(2) | 5.662(2) | 5.110(9) |
| $Q_{multipole}$ (Co)<br>$Q_{multipole}$ (Sb) | -0.047(4),<br>+0.016(1) | -0.062(5),<br>+0.021(2) | +1.979(7),<br>-0.659(2) | +1.988(6),<br>-0.662(2) | +0.33(3),<br>-0.110(9) |
| $Q_{ATB}$(Co) | -0.49 | -0.49 | 0.05 | 0.02 | -0.35 |
| $Q_{ATB}$(Sb) | 0.18 | 0.18 | -0.00 | -0.01 | 0.13 |
| $\rho$, $\nabla^2\rho$ (Co-Sb) | 0.426, 1.539 | 0.426, 1.543 | 0.423, 1.917 | 0.423, 1.870 | 0.420, 1.667 |
| $AIL_{Co\text{-}BCP}$, $AIL_{Sb\text{-}BCP}$ | 1.181, 1.343 | 1.182, 1.342 | 1.130, 1.394 | 1.132, 1.392 | 1.156, 1.368 |
| $\rho$, $\nabla^2\rho$ (Sb-Sb1) | 0.378, 0.166 | 0.378, 0.156 | 0.390, 0.096 | 0.391, 0.062 | 0.382, 0.130 |
| $AIL_{Sb\text{-}BCP}$ | 1.424 | 1.424 | 1.424 | 1.424 | 1.424 |
| $\rho$, $\nabla^2\rho$ (Sb-Sb2) | 0.316, 0.328 | 0.317, 0.316 | 0.328, 0.231 | 0.329, 0.197 | 0.319, 0.291 |
| $AIL_{Sb\text{-}BCP}$ | 1.486 | 1.487 | 1.487 | 1.487 | 1.487 |

**Table S4.b:** Results from multipole refinements against the experimental SPring8 data. The refinements are based on $F^2$. The five different models are tested, all with $\kappa$ and $\kappa'$ fixed (KKRMM) at the values obtained for the corresponding models from theory in Table S4, a).

| **SPring8, KKRMM** | **Model 1** | **Model 2** | **Model 3** | **Model 4** | **Model 5** |
|---|---|---|---|---|---|
| $R(F^2)$ | 1.27 % | 1.27 % | 1.30 % | 1.29 % | 1.27 % |
| $\pm\Delta\rho$ (e/Å$^3$) | -1.81/7.85 | -1.80/7.84 | -1.82/7.88 | -1.82/7.88 | -1.80/7.81 |
| $^{2nd}\Delta\rho_{max}$ (e/Å$^3$) | 2.41 | 2.41 | 2.46 | 2.44 | 2.41 |
| $\pm\Delta\rho$ (e/Å$^3$) s<0.8 | 1.86/-0.46 | 1.86/-0.46 | 1.89/-0.47 | 1.88/-0.46 | 1.84/-0.47 |
| $^{2nd}\Delta\rho_{max}$ (e/Å$^3$) s<0.8 | 0.53 | 0.52 | 0.56 | 0.55 | 0.51 |
| $\kappa$ (Co, 4*s*) theory | 1 | - | - | - | 0.988 |
| $\kappa$, $\kappa'$ (Co) theory | 0.992, 1.020 | 0.991, 1.367 | 0.998, 1.012 | 0.999, 1.015 | 0.993, 1.036 |
| $\kappa$, $\kappa'$ (Sb) theory | 0.979, 0.803 | 0.979, 0.798 | 0.951, 0.747 | 0.965, 0.757 | 0.9735, 0.791 |
| $P_{val}$(Co), $P_{val}$(4s) | 7.5(1) | 9.6(1) | 7.5(1) | 7.5(1) | 7.4(1), 2.6(9) |
| $P_{val}$(Sb) | 4.85(4) | 4.80(4) | 5.51(4) | 5.51(4) | 4.7(3) |
| $Q_{multipole}$ (Co)<br>$Q_{multipole}$ (Sb) | -0.5(1)<br>+0.15(4) | -0.6(1)<br>0.20(4) | 1.5(1)<br>-0.51(4) | 1.5(1)<br>-0.51(4) | -0.9(10)<br>+0.3(3) |
| $Q_{ATB}$(Co) | -0.63 | -0.67 | -0.07 | -0.09 | -0.84 |
| $Q_{ATB}$(Sb) | 0.22 | 0.24 | 0.04 | 0.05 | 0.29 |
| $\rho$, $\nabla^2\rho$ (Co-Sb) | 0.395, 1.709 | 0.394, 1.719 | 0.388, 2.070 | 0.388, 2.029 | 0.386, 1.696 |
| $AIL_{Co\text{-}BCP}$, $AIL_{Sb\text{-}BCP}$ | 1.193, 1.331 | 1.196, 1.328 | 1.136, 1.391 | 1.138, 1.389 | 1.191, 1.334 |
| $\rho$, $\nabla^2\rho$ (Sb-Sb1) | 0.402, 0.197 | 0.405, 0.165 | 0.368, 0.681 | 0.370, 0.633 | 0.427, -0.102 |
| $AIL_{Sb\text{-}BCP}$ | 1.442 | 1.442 | 1.444 | 1.444 | 1.446 |
| $\rho$, $\nabla^2\rho$ (Sb-Sb2) | 0.330, 0.212 | 0.332, 0.185 | 0.320, 0.499 | 0.320, 0.473 | 0.345, 0.010 |
| $AIL_{Sb\text{-}BCP}$ | 1.493 | 1.493 | 1.493 | 1.493 | 1.494 |

**Table S4.c:** Results from multipole refinements against the experimental SPring8 data. The refinements are performed on $F^2$. The five different models are tested, all with freely refined $\kappa$ and $\kappa'$ (UMM).

| **SPring8, UMM** | **Model 1** | **Model 2** | **Model 3** | **Model 4**[¤] | **Model 5** |
|---|---|---|---|---|---|
| $R(F^2)$ | 1.34 % | 1.35 % | 1.38 % | 1.38 % | 1.36 % |
| $\pm\Delta\rho$ (e/Å$^3$) | -1.78/+8.04 | -1.78/+8.03 | -1.79/+8.09 | -1.78/+8.10 | -1.79/+8.03 |
| $^{2nd}\Delta\rho_{max}$ (e/Å$^3$) | 2.27 | 2.26 | 2.29 | 2.29 | 2.22 |
| $\pm\Delta\rho$ (e/Å$^3$) *s<0.8* | -0.44/2.04 | -0.44/+2.04 | -0.43/+2.10 | -0.43/+2.09 | -0.45/+2.02 |
| $^{2nd}\Delta\rho_{max}$ (e/Å$^3$) *s<0.8* | 0.64 | 0.64 | 0.68 | 0.67 | 0.64 |
| $\kappa$ (Co, 4s) | 1 | - | - | - | 1.2(1) |
| $\kappa$, $\kappa'$ (Co) | 1.02(1), 0.74(7) | 1.02(1), 0.99(9) | 1.03(1), 0.73(7) | 1.03(1), 1.015 | 1.01(1), 1.035(0) |
| $\kappa$, $\kappa'$ (Sb) | 1.09(3), 0.69(6) | 1.10(3), 0.69(7) | 1.07(3), 0.67(5) | 1.09(3), 0.69(5) | 1.12(3) , 0.73(9) |
| $P_{val}$(Co), $P_{val}$(4s) | 7.1(2) | 9.1(3) | 7.0(2) | 7.0(2) | 7.2(2), 2.4(1) |
| $P_{val}$(Sb) | 4.97(7) | 4.96(9) | 5.68(7) | 5.68(7) | 4.8(3) |
| $Q_{multipole}$ (Co)<br>$Q_{multipole}$ (Sb) | -0.1(9)<br>0.03(7) | -0.1(3)<br>0.04(9) | 2.0(2)<br>-0.68(7) | 2.0(2)<br>-0.67(7) | -0.6(3)<br>+0.2(3) |
| $Q_{ATB}$(Co) | -0.59 | -0.59 | -0.16 | -0.20 | -0.74 |
| $Q_{ATB}$(Sb) | 0.20 | 0.20 | 0.06 | 0.07 | 0.25 |
| $\rho$, $\nabla^2\rho$ (Co-Sb) | 0.421, 1.468 | 0.422, 1.472 | 0.426, 1.728 | 0.425, 1.978 | 0.388, 2.288 |
| $AIL_{Co\text{-}BCP}$, $AIL_{Sb\text{-}BCP}$ | 1.156, 1.369 | 1.167, 1.359 | 1.118, 1.411 | 1.133, 1.396 | 1.196, 1.328 |
| $\rho$, $\nabla^2\rho$ (Sb-Sb1) | 0.370, 0.661 | 0.369, 0.678 | 0.335, 1.196 | 0.335, 1.174 | 0.382, 0.537 |
| $AIL_{Sb\text{-}BCP}$ | 1.447 | 1.447 | 1.452 | 1.450 | 1.445 |
| $\rho$, $\nabla^2\rho$ (Sb-Sb2) | 0.386, -0.083 | 0.384, -0.071 | 0.391, 0.189 | 0.388, 0.188 | 0.368, -0.028 |
| $AIL_{Sb\text{-}BCP}$ | 1.488 | 1.488 | 1.487 | 1.487 | 1.490 |

[¤] $\kappa'$ for Co has been fixed at the values obtain from theory, Model 4 in order to obtain convergence.

***Core polarization***

The highest residual density peaks from the fitting of the multipole model to the theoretical data are found in the core regions of Co and Sb. There can be several explanations for this observation: Aspherical features can arise in the core region due to an incorrect (radial) description of the *valence* electrons. It might also be that the features are caused by a deformation (contraction/expansion and potentially polarization) of the core density of the atoms in the crystal that is not present for the atoms in the gas phase. In any case, this so-called core-polarization can be taken into account by refining radial and multipole parameters for some of the core shells. The presence of core polarization effects in electron densities from multipole refinement against theoretical data has previously been observed (Fischer *et al.*, 2011. Overgaard *et al.*, 2011).

Introducing additional sets of multipolar functions for the core shells of each pseudoatom in order to describe any potential core-polarization yielded an even better fit to the theoretical structure factors as shown below. Only values of parameters related to the valence density are shown.

**Table S5.** Results of multipole refinements against the theoretical data including additional sets of multipolar functions for the core shells of each pseudoatom in order to describe any potential core-polarization. Only values of parameters related to the valence density are shown. $\kappa'$ for Sb and Co are fixed at the values obtained from fitting Model 5 (Table S4. a) to the theoretical data in order to obtain convergence.

| | |
|---|---|
| $R(F)$ | 0.01 % |
| $\pm\Delta\rho$ (e/Å$^3$) | -0.023/0.022 |
| $\kappa$ (Co, 4*s*) | 0.970(2) |
| $\kappa$, $\kappa'$ (Co, 3*d*) | 0.9954(4), 1.036 |
| $\kappa$, $\kappa'$ (Sb) | 0.9735(3), 0.791 |
| $P_{val}$(Co), $P_{val}$(*4s*) | 7.032(2), 1.80(2) |
| $P_{val}$(Sb) | 5.055(7) |
| $Q_{multipole}$ (*Co*) | +0.19(2) |
| $Q_{multipole}$ (*Sb*) | -0.055(7) |

**Figure S9.** Residual density plots in the $CoSb_4$ plane (left) and the $Sb_4$ plane (right) for the theoretical data fitted against a model including core polarization. The step size is 0.01 e/Å$^3$. Full, blue contours are positive. Dashed, red contours are negative.

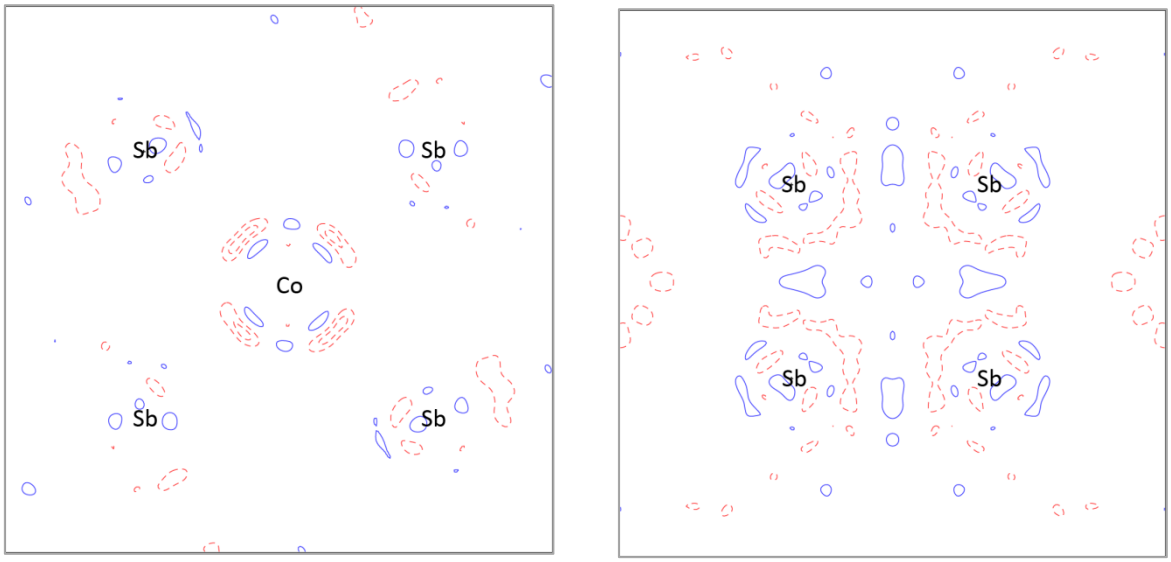


**Figure S10.** Three-dimensional Laplacian distribution of Co from the theoretical data fitted to the model including core polarization. The contour level is -800 e/Å$^5$.